Research Article | Vol. 11, No. 1 / 1 January 2020 / Biomedical Optics Express 227
Biomedical Optics EXPRESS

Gabor optical coherence tomographic angiography (GOCTA) (Part II): theoretical basis of sensitivity improvement and optimization for processing speed

CHAOLIANG CHEN,[1] WEISONG SHI,[1,2] JOEL RAMJIST,[1] AND VICTOR X. D. YANG[1,3,4,*]

[1]*Biophotonics and Bioengineering Lab, Department of Electrical, Computer, and Biomedical Engineering, Ryerson University, Toronto, Ontario, Canada*
[2]*Department of Optical Engineering, Nanjing University of Science and Technology, Nanjing, Jiangsu, China*
[3]*Division of Neurosurgery, Sunnybrook Health Sciences Centre, Toronto, Ontario, Canada*
[4]*Division of Neurosurgery, Faculty of Medicine, University of Toronto, Toronto, Ontario, Canada*
[*]*yangv@ryerson.ca*

Abstract: We previously proposed a Gabor optical coherence tomography angiography (GOCTA) algorithm for spectral domain optical coherence tomography (SDOCT) to extract microvascular signals from spectral fringes directly, with speed improvement of 4 to 20 times over existing methods. In this manuscript, we explored the theoretical basis of GOCTA with comparison of experimental data using solid and liquid displacement sample targets, demonstrating that the majority of the GOCTA sensitivity advantage over speckle variance based techniques was in the small displacement range ($< 10 \sim 20\,\mu m$) of the moving target (such as red blood cells). We further normalized GOCTA signal by root-mean-square (RMS) of original fringes, achieving a more uniform image quality, especially at edges of blood vessels where slow flow could occur. Furthermore, by transecting the spectral fringes and using skipped convolution, the data processing speed could be further improved. We quantified the trade-off in signal-to-noise-ratio (SNR) and contrast-to-noise-ratio (CNR) under various sub-spectral bands and found an optimized condition using 1/4 spectral band for minimal angiography image quality degradation, yet achieving a further 26.7 and 34 times speed improvement on GPU and CPU, respectively. Our optimized GOCTA algorithm has a speed advantage of over 140 times compared to existing speckle variance OCT (SVOCT) method.

1. Introduction

Optical coherence tomography (OCT) [1] technique, proposed in 1990's, is an emerging imaging modality for medical diagnostics and treatment monitoring. Due to the advantages of non-invasiveness, high resolution and high imaging speed, OCT has been used for various tissues, e.g. human retina, brain, cardiology, and dermatology. In addition to microstructural imaging, functional OCTs (such as optical Doppler tomography (ODT) [2,3] or color Doppler OCT (CDOCT) [4]) have been presented to measure the velocity of red blood cells in clinical applications.

Besides Doppler based algorithms, a variety of phase, amplitude or complex signals based OCT angiographic (OCTA) algorithms have also been proposed to contrast microvasculature, where higher contrast can be achieved but the velocity information is ignored. In general, there are two categories of OCTA algorithms according to the processing modes. The first is inter-line mode, such as Doppler variance phase resolved (DVPR) [3,5], intensity-based modified Doppler variance (IBDV) [6], and optical micro-angiography (OMAG) [7]. High A-scan density is usually needed

#380287 https://doi.org/10.1364/BOE.380287
Journal © 2020 Received 17 Oct 2019; revised 5 Dec 2019; accepted 5 Dec 2019; published 11 Dec 2019

Biomedical Optics EXPRESS

by this mode since the dynamic signal is extracted from background by using a few consecutive A-scans. The other mode is inter-frame, such as phase variance OCT (PVOCT) [8], speckle variance OCT (SVOCT) [9–12], correlation mapping OCT (cmOCT) [13–15], split-spectrum amplitude-decorrelation angiography (SSADA) [16], differential standard deviation of log-scale intensity (DSDLI) [17], and ultrahigh sensitivity optical micro-angiography (UHS-OMAG) [18–19]. For this mode, vascular information is extracted by comparing the two A-scans (from the same position) acquired at different time. The sensitivity for detecting dynamic signals can be improved compared to the first mode since the time interval between the 2 A-scans is increased.

One of the major research directions in the OCT field is parallel imaging or high A-scan [20–22] speed and wide-field scanning [23], in which the acquired large quantity of data poses a challenge for real-time data processing. To solve this problem, we previously proposed a Gabor optical coherence tomographic angiography (GOCTA) algorithm [24] to improve the data processing speed of calculating *en face* blood flow images. In this manuscript, we explored the theoretical basis of GOCTA and identified normalization technique to obtain more uniform GOCTA signal. Furthermore, the data processing speed was vastly improved by using a subset of SDOCT fringe data and skipped convolution without significant degradation of image quality.

2. Theory and method

2.1. Theory and simulation

In SDOCT, the light back from sample and reference arms interferes and the fringe can be expressed by [25]

$$I(\lambda) = S(\lambda)R_s \cos\left(\frac{4\pi}{\lambda}nz + \phi_0\right), \tag{1}$$

where λ is wavelength, $S(\lambda)$ is power spectral density of light source, R_s is the backscattering coefficient of sample, n and z are the refractive index and depth of sample, and ϕ_0 is the initial phase. When the scattering particle moves, the scattering coefficient or particle's depth may change, resulting in the variance of amplitude or phase signals versus time. Based on this fact, a couple of B-scans can be acquired at the same position for OCTA calculation. To preserve the scanning speed, only two B-scans are acquired for GOCTA. To calculate dynamic signals, the first step is to calculate the differential fringe, expressed by

$$Id(\lambda) = I_1(\lambda) - I_2(\lambda). \tag{2}$$

Because the sample information at different depths is modulated by different frequency components of the fringes and Gabor filter is a linear filter which can be used to extract the components within a frequency range, the new differential fringes $Id'(\lambda)$ from a specific depth-range can then be obtained for *en face* vascular images calculation by convolving the Gabor filters (generated with sample surface information) with the original differential fringes [24]. Note that the Gabor filters are one dimensional and performed in depth direction. In our previous work, GOCTA signal is calculated by [24]

$$GOCTA = \sqrt{\frac{1}{M}\sum_{n=1}^{M}[Id'(\lambda_n) - Id'_{mean}]^2}. \tag{3}$$

During OCT scanning, the backscattered light intensity by sample may vary due to speckle effect, surface incline, refraction, and shadowing from vessels, which can modulate the background of GOCTA image. Therefore, we divide the obtained GOCTA signal by root-mean-square (RMS) of the original fringes to improve uniformity, and the optimized (GOCTA') signals can be expressed

Biomedical Optics EXPRESS

by

$$GOCTA' = \frac{GOCTA}{\sqrt{\frac{1}{M}\sum_{n=1}^{M} I_1(\lambda_n)^2}} = \sqrt{\frac{\sum_{n=1}^{M} [Id'(\lambda_n) - Id'_{mean}]^2}{\sum_{n=1}^{M} I_1(\lambda_n)^2}}. \quad (4)$$

We numerically simulated GOCTA' signals at different flow speed, characterized by different displacements between interference spectra measurements, and compared them to corresponding SVOCT signals. The results are shown in Fig. 1, where we assumed a Fourier domain OCT system with center wavelength of 1310 nm and a bandwidth of 100 nm with normalized optical power spectral density shown in Fig. 1(a). A moving scattering particle produced two interference spectra, marked red and blue as shown in Fig. 1(b), where the difference between them was the basis of GOCTA signal. At small displacements between spectral measurements, there was an oscillating pattern of the difference between the interference fringes, as shown in Fig. 1(c), with diminishing amplitude which approached the limit of SVOCT as displacement increased. Ideally, the improvement of GOCTA' over SVOCT was primarily at small flow speed, where there was small target displacements between interference spectra measurements, as shown in Fig. 1(d) which was obtained by dividing the red curve (GOCTA data) by black curve (SVOCT data) in Fig. 1(c) and expressed in dB. In addition, the simulation represented a single scatterer's response. Multiple scatterers within the focal volume, each with different speed (and therefore different displacements), would result in an ensemble with reduced overall improvement. Hence, we anticipated there could be a sensitivity advantage of GOCTA' over SVOCT at slow flow speed, or small displacement between interference spectra measurements.

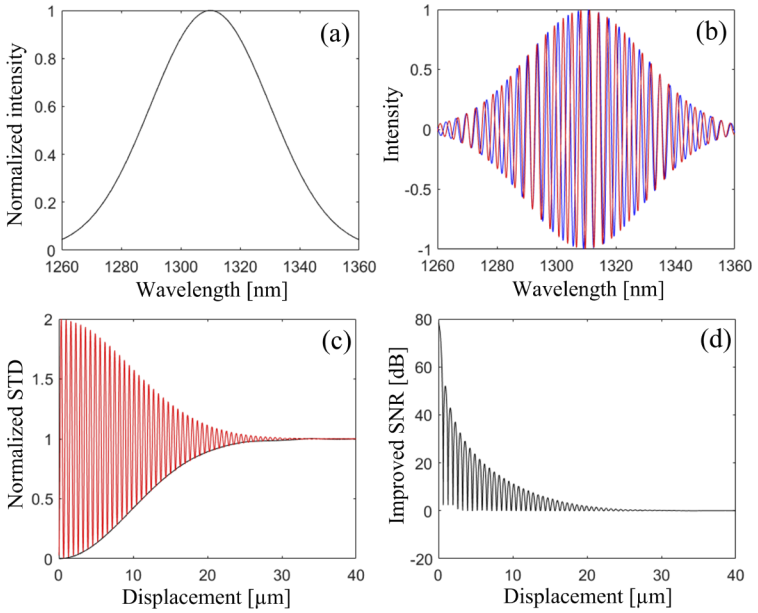

Fig. 1. Simulation results. (a) Normalized optical power spectral density. (b) Two A-scans of fringes with different displacements. (c) Plots of GOCTA' (red) and SVOCT (black) signals versus different displacements of moving particles. (d) Plot of the improved SNR versus displacements for GOCTA' compared to SVOCT.

We first verified the simulation result using a solid displacement target. A slightly tilted mirror was used as the sample (illustrated in Fig. 2(a)). As the galvo swept the sample beam across the

Biomedical Optics EXPRESS

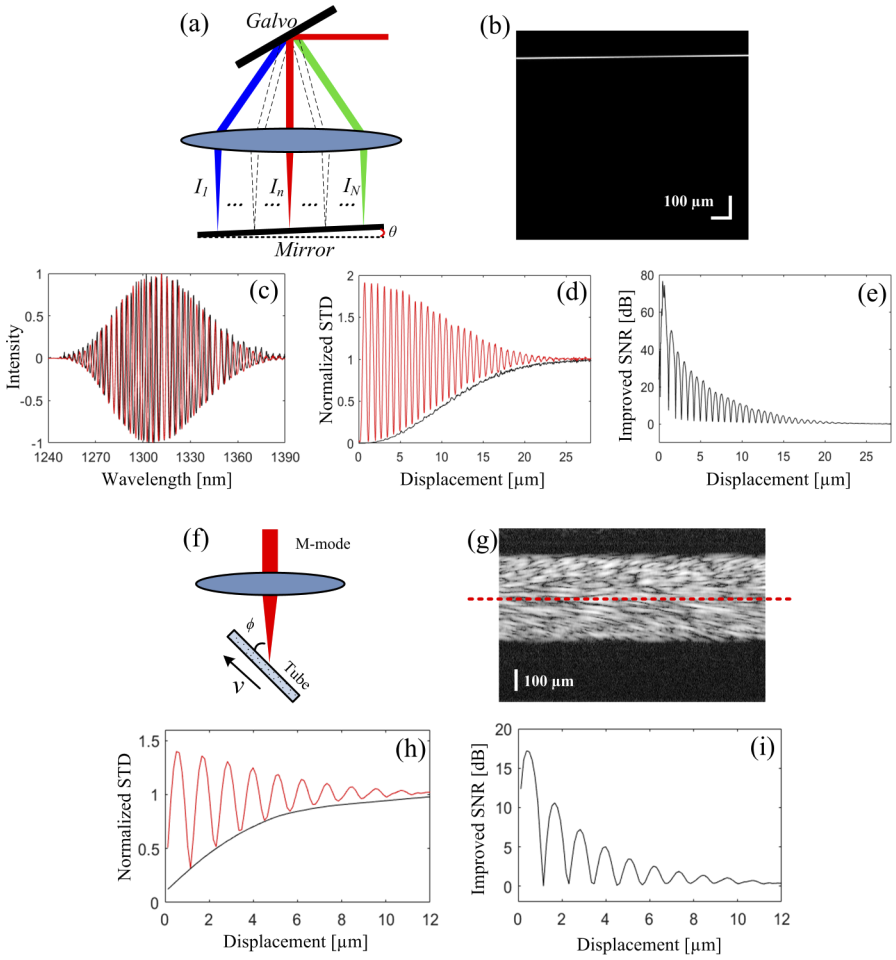

Fig. 2. Solid and liquid phantom verification experiments. (a) Tilted mirror target with galvo in sample arm to generate reproducible displacements between A-scans. (b) Structural image of all A-scans. (c) Interference fringes of two example A-scans with displacement of 6.9 μm. (d) Plots of the calculated GOCTA' signals (red) and SVOCT signals (black) versus displacements. (e) Improved SNR of GOCTA' compared to SVOCT obtained by dividing red curve by black curve in (d). (f) Illustration of experimental settings of flow phantom. (g) M-mode (structural) image of A-scans. (h) Plots of the calculated GOCTA' signals (red) and SVOCT signals (black) versus displacements using the OCT signal marked by dashed red line in (g). (i) Improved SNR achieved by GOCTA' compared to SVOCT.

tilted mirror, different small axial displacements could be created (by comparing each A-scan to the first A-scan) for the analysis of the performance of GOCTA'. The fringes were acquired by a home-built SDOCT system which included a superluminescent diode (SLD) with a center wavelength of 1310 nm and a bandwidth of 60 nm (giving an axial resolution of 12.6 μm in air). In the sample arm, the diameter of collimated beam was 3.4 mm, and the objective lens had a focal length of 30 mm, giving a lateral resolution of 8.6 μm. The spectrometer was based on a grating (with a frequency of 892 lines/mm), achieving a spectral resolution of 0.365 nm. An InGaAs camera (Goodrich SU-LDH2, Sensors Unlimited) with 1024 pixels was used to detect optical interference fringes at its maximum A-scan rate of 91,912 Hz. In this way, the interference spectra with small displacements could be obtained and the corresponding structural

Biomedical Optics EXPRESS

image was shown in Fig. 2(b). By comparing each A-scan (I_n) to the first A-scan (I_1), the plots of GOCTA' and corresponding SVOCT signals versus displacements were obtained and shown in Fig. 2(d), demonstrating similarity to Fig. 1(c) as predicted by simulation. Figure 2(e) showed the improvement (expressed in dB) achieved by GOCTA' over SVOCT.

While the tilted mirror target experiment provided excellent agreement with simulation, we would like to explore tissue mimicking 1% intralipid solution at room temperature as liquid flow phantom for experimental validation of GOCTA', with multiple scatterers inside the focal volume. As shown in Fig. 2(f), a plastic tube with an inner diameter of 0.28 mm was positioned at 60° Doppler angle, through which the intralipid solution was pumped with a mean velocity of 18.5 mm/s by a syringe pump (Harvard Apparatus, Holliston, MA). We operated the SDOCT system in M-mode and the structural image was shown in Fig. 2(g). Since the velocity varied along the depth direction, the intereference signal at the center of tube marked by the dashed red line was obtained to calculate GOCTA' and SVOCT signals, as shown in Fig. 2(h). Since the intralipid particles had aggregate sizes smaller than the focal volume, multiple scatterers, each with potentially different individual movement speed, produced an ensemble effect on the GOCTA' signal with reduced oscillating amplitude in Fig. 2(h). As shown in Fig. 2(i), there was still up to 17 dB of improvement over SVOCT at slow flow speed, since GOCTA' used both amplitude and phase from interference fringes to extract dynamic information, while only structural OCT signal amplitude was used in SVOCT. We noted the horizontal axes in Fig. 2(h) and (i) represented only the bulk flow related displacement, which would be an underestimate of intralipid particle movement which were subjected to other effects such as Brownian motion and turbulence. For simplicity, we did not take their contribution as well as the ensemble effect into consideration for our simulation. Nevertheless, the intralipid flow phantom experiment demonstrated improvement of GOCTA' over SVOCT based technique, which provided basis for the subsequent human retinal imaging experiments.

2.2. Optimization of data processing speed

We previously used simple spherical approximation for the human retinal surface, where a fixed radius of curvature determined from healthy population and 3 A-scans provided the input parameters for the approximation [24]. For the optic nerve head region, and to a lesser extent, the fovea, complex surface contours existed, which demanded refinement for the surface contour extraction. Here we employed a sparse 9×9 matrix of A-scans, with limited computational penalty (see Fig. 3(a)) for performing FFT and 2D cubic interpolation, to allow more precise determination of the retinal surface. For more uniform regions, the matrix density can be reduced further.

Since power spectral density of SLD was approximately a Gaussian function where the central part of spectrum carries the majority of sample information, the spectral fringes obtained by OCT detecting system could be truncated to decrease computation complexity without significant degradation of image quality (Fig. 3(b)), achieving a higher data processing speed. Based on the fact that all pixels in spectral fringes carried the information of moving scatterers, skipped convolution could be performed to further decrease computational complexity. As shown in Fig. 3(c), the Gabor filter kernel shifted along A-scan direction and did multiplication and summation with the same number of pixels. After each round of calculation, the kernel went to the next set of pixels without overlapping pixels for the next round of calculation. In this way, each pixel was only used once for calculation, while each pixel was used N_g (size of Gabor filter kernel) times for calculation in standard convolution. Therefore, computational complexity could be significantly decreased with skipped convolution compared to standard convolution. This effect was clearly tabulated in Table 1, where we analyzed the computational complexity in terms of the number of multiplications and summations used in FFT or skipped convolution, for full spectral band, 1/2, and 1/4 truncated spectral bands. Note the convolution kernel length (N_g) for

Biomedical Optics EXPRESS

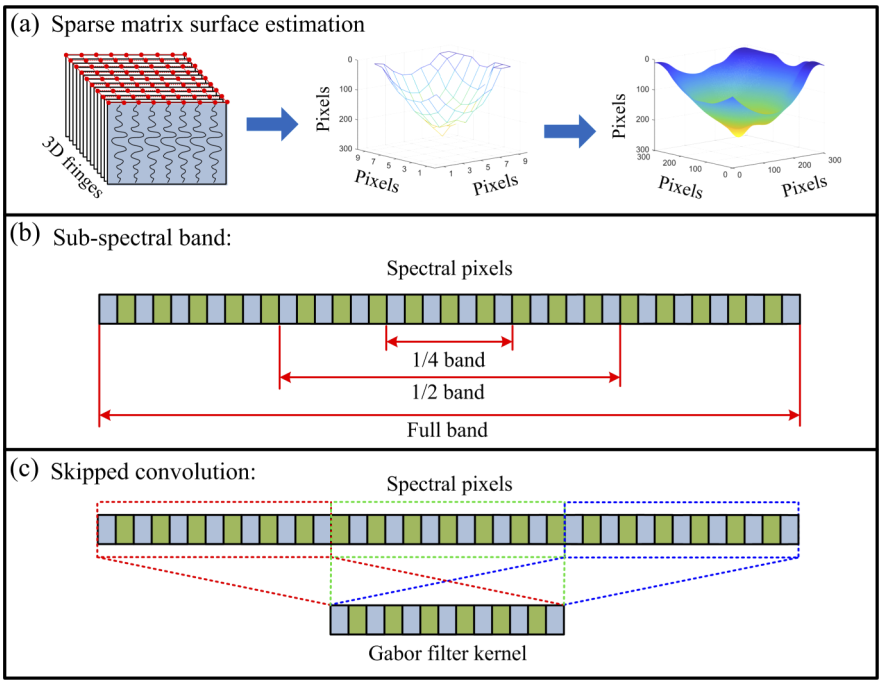

Fig. 3. Sparse matrix surface estimation (a), sub-spectral band (b), and skipped convolution for GOCTA' (c).

GOCTA' was kept at 16. If the spectral band could be truncated to 1/4 bandwidth, then only approximately 5% of the multiplications and 2% of the summations needed to be computed, providing dramatic speed improvement over FFT using the full spectrum. The trade-off in OCTA image quality needed to be examined experimentally using human volunteers in retinal imaging, which would be described in the next section.

Table 1. Comparison of computational complexity of FFT vs skipped convolution in each A-scan

# of operations	Operation type	Full spectral band	1/2 spectral band	1/4 spectral band
FFT	Multiplication	11264	5120	2304
	Summation	22528	10240	4608
Skipped convolution	Multiplication	2048	1024	512
	Summation	1920	960	480

3. Experimental results

3.1. OCT system

As reported in our previous paper [24], all *in vivo* experiments were performed on a commercial SDOCT system (AngioVue, OptoVue Inc.). This system operated at a center wavelength of 840 nm with the axial resolution and lateral resolution of ~5 μm and ~15 μm, respectively. The A-scan rate was 70,000 A-scans per second and each A-scan contained 2048 pixels. 304× 2×304 A-scans were acquired for each dataset covering 3×3 mm^2 (9.9 μm of A-scan interval) and each position was scanned twice for OCTA information extraction.

Biomedical Optics EXPRESS

3.2. Comparison of optimized GOCTA' images with different spectral bands and skipped convolution

To test the performance of the optimized GOCTA', we scanned the optical nerve head region (3×3 mm^2) of a female healthy volunteer's retina and calculated *en face* vascular images with different spectral bands using both regular convolution and skipped convolution for comparison (Fig. 4). Comparing Fig. 4(a)–(f), it could be seen that the image quality of GOCTA' images with different spectral bands and with skipped convolution was comparable.

Similar to our previous work [24], a mask obtained by thresholding the averaged image was used to calculate SNRs and CNRs for quantitative comparison, as shown in Fig. 4(h) and Fig. 4(i).

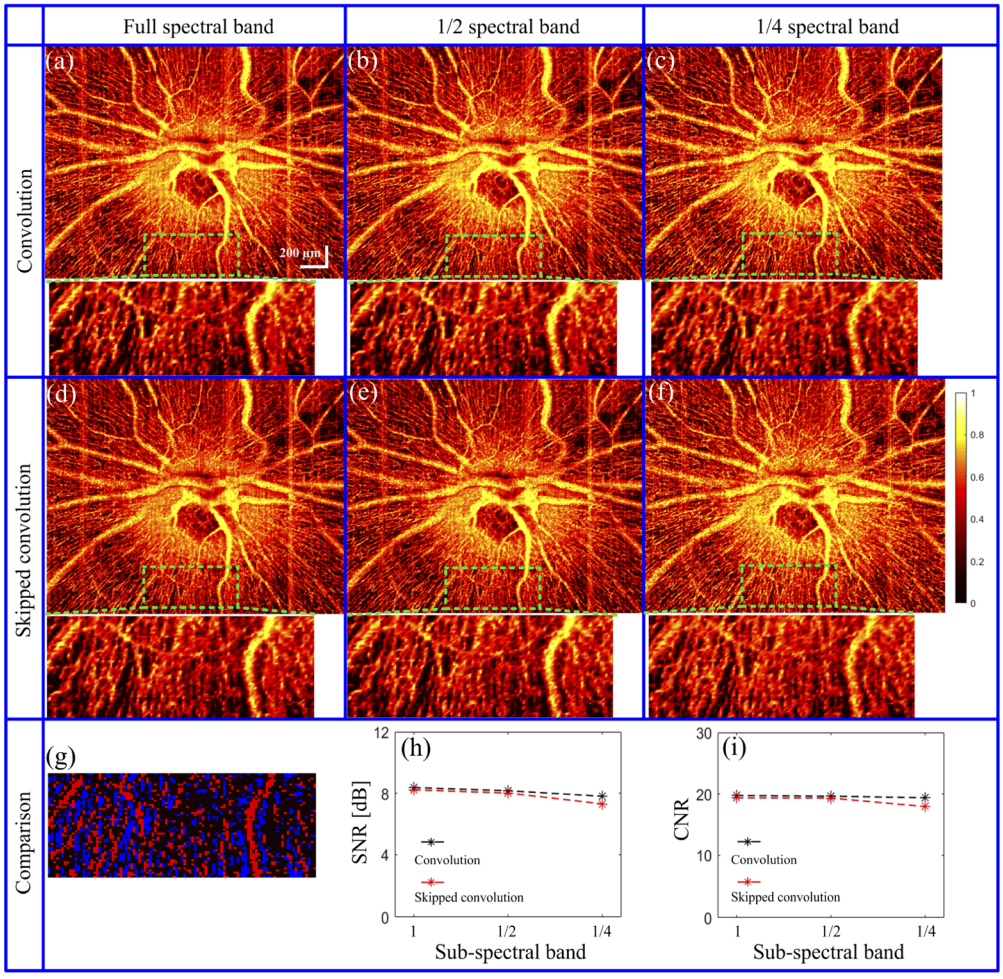

Fig. 4. Comparison of GOCTA' images with different spectral bands and skipped convolution. (a)–(c) GOCTA' images with different spectral bands obtained by regular convolution. (d)–(f) GOCTA' images with different spectral bands obtained by skipped convolution. (g) Mask of dynamic vascular signals (red) and static signals (blue) in the magnified local region in (a)–(f) for SNR calculation. (h)–(i) Calculated SNR and CNR plots versus different spectral bands. The depth-range of 0–170 μm below surface is used for (a)–(f) and (a)–(f) share the same scale bar.

Biomedical Optics EXPRESS

The SNR and CNR are calculated by

$$SNR = 20 \cdot \log[(\bar{I}_{sig} - \bar{I}_{bkg}) / \sigma_{bkg}], \tag{5}$$

and

$$CNR = (\bar{I}_{sig} - \bar{I}_{bkg}) \Big/ \sqrt{(\sigma_{sig}^2 + \sigma_{bkg}^2) / 2}, \tag{6}$$

where $\bar{I}_{sig}$ and $\bar{I}_{bkg}$ are the mean value of the vascular intensities and background intensities, σ_{sig} and σ_{bkg} are the standard deviation of vascular and background intensities. It can be seen that only 1.8 dB (SNR) and 1.1 (CNR) degradations were caused by truncating to 1/4 spectral band and using skipped convolution.

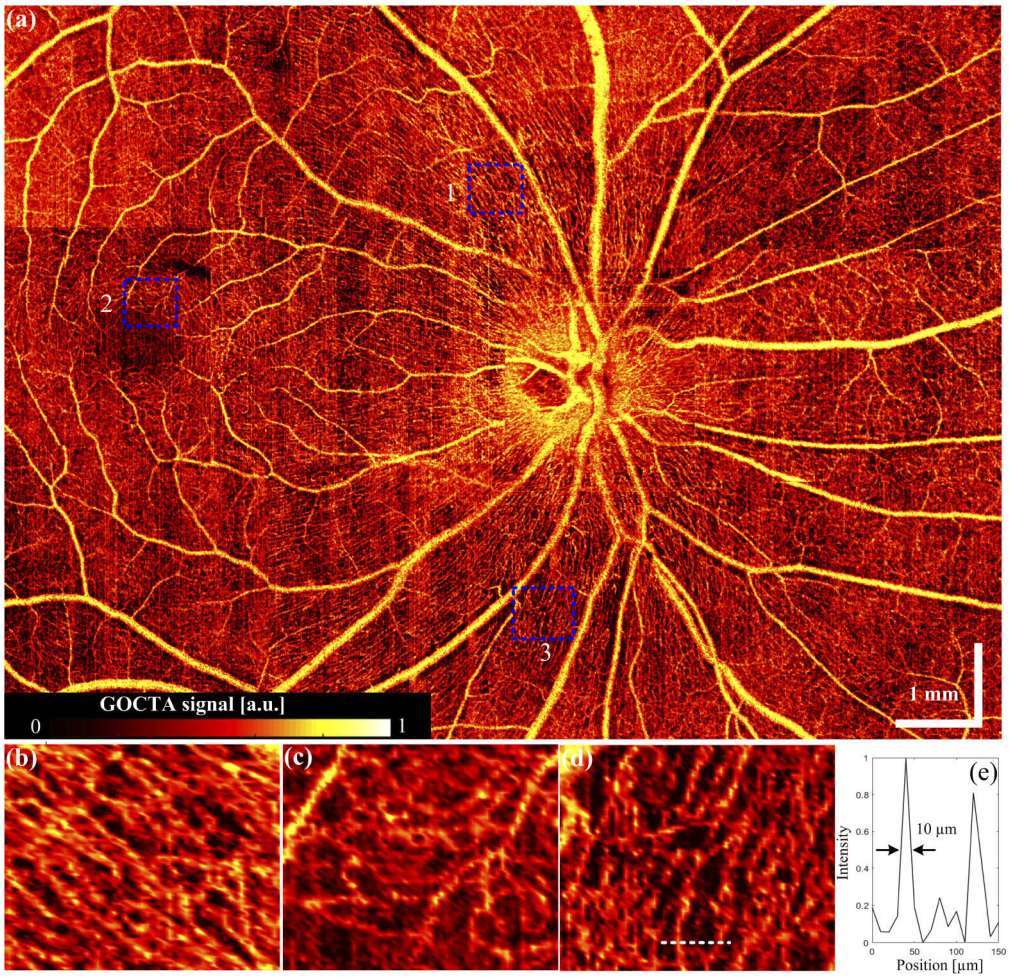

Fig. 5. (a) Mosaic retinal image of a healthy female (23 years old) volunteer's left eye obtained by GOCTA' with 1/4 spectral band and skipped convolution. (b)–(d) Magnified images of the marked regions by dashed blue rectangles 1–3. (d) The plot of pixel values at the marked position by a dashed white line in (d). The depth-range of 0–170 µm (with tissue refractive index of 1.35) below surface is used.

Biomedical Optics EXPRESS

To test whether such degradations would impact image quality, especially for identification of small blood vessels, we scanned a mosaic of 12 local regions (each at 3×3 mm^2 size) on the same volunteer's retinal surface. The result was shown in Fig. 5.

3.3. Comparison of GOCTA' with SVOCT on both image quality and processing time

To verify the theory of better contrast can be achieved by GOCTA' compared to SVOCT, fovea region on the other eye of the same volunteer was scanned and processed for comparison, the results are shown in Fig. 6. The SVOCT images with full spectral band and 1/4 spectral band were both calculated and shown for comparison. Three local regions (marked by green rectangles) were used to calculate SNR and CNR for quantitative comparison. Take Region 1 (magnified) as an example, a mask for vascular signals and background signals was first obtained by thresholding the local region. SNR and CNR could then be calculated using Eq. (5) and Eq. (6). The SNRs for Region 1 - 3 are 10.3, 9.5, 8.3 dB for GOCTA' with 1/4 spectral band, 9.6, 9.0, 8.0 dB for SVOCT with full spectral band, and 8.4, 7.6, 6.9 dB for SVOCT with 1/4 spectral band. The CNRs for Region 1 - 3 are 2.2, 2.1, 2.2 for GOCTA' with 1/4 spectral band, 2.1, 2.1, 2.1 for SVOCT with full spectral band, and 1.9, 1.9, 1.8 for SVOCT with 1/4 spectral band. The average SNR and CNR of the three regions are 9.4, 8.9, 7.6 dB and 2.2, 2.1, 1.9, respectively. We can see that GOCTA' with 1/4 spectral band and skipped convolution could provide comparable SNR and CNR to SVOCT with full spectral band, and higher SNR and CNR than SVOCT with 1/4 spectral band.

We also compared the GOCTA' imaging with SVOCT for the optic nerve head region, where both large and small vessels were present (Fig. 7). The GOCTA' algorithm provided more uniform signal across both large and small vessels, with the difference image between it and SVOCT showed more microvasculature in and around the lamina cribrosa.

To quantify the speed advantage of using sub-spectral band and skipped convolution for GOCTA' analysis, we measured the data processing time on both CPU and GPU and compared to data processing time of SVOCT with full spectral band and 1/4 spectral band. For both algorithms, data processing was performed on the same laptop (CPU: i7-4720HQ, memory: 16 GB, GPU: NVIDIA Geforce GTX 970M, operating system: windows 8.1), and CPU processing time and GPU processing time were measured in MATLAB and CUDA, respectively. The data processing time on CPU and GPU for each two B-scans was shown in Table 2. Note that surface calculation was performed on CPU for both scenarios and the time for surface calculation was obtained through dividing the entire time by the scanning steps in slow scanning direction. To improve the accuracy of time measurement, the processing times for each step shown in Table 2 were the average processing time of 100 pairs of B-scans.

Table 2. Data processing time of each pair of B-scans for GOCTA' with 1/4 spectral band and skipped convolution on CPU and GPU

	3D data processing time (ms)							
	Surface calculation	Data transfer	Preparation	Subtraction	Skipped convolution	STD	RMS	Total
CPU	0.11	-	-	0.33	1.59	0.10	0.64	2.77
GPU	0.11	0.13	0.14	0.01	0.44	0.01	0.02	0.86

We also measured the processing time for entire 3D dataset on CPU and GPU, respectively, for comparison and the results are shown in Table 3. By using 1/4 spectral band and skipped convolution, the GOCTA' processing speed for 3D dataset can be improved by almost 144 and 30 times than SVOCT with full spectral band and 1/4 spectral band on CPU, respectively. For SVOCT, the majority of data processing time is for k-space re-sampling [24], which was performed by spline fitting.

Biomedical Optics EXPRESS

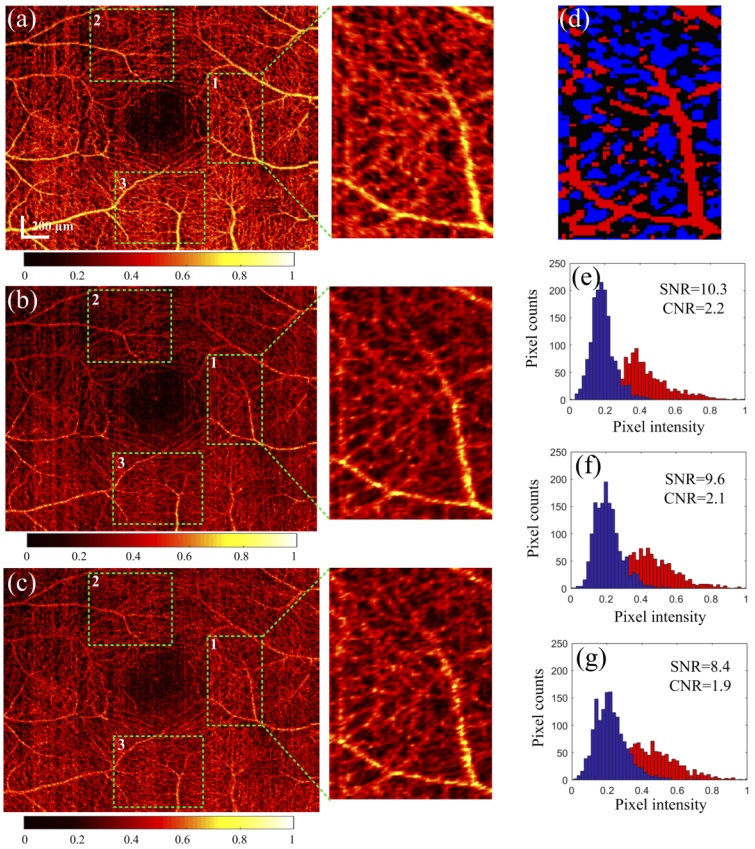

Fig. 6. Comparison of GOCTA' image with SVOCT images of fovea. (a) GOCTA' images with 1/4 spectral band and skipped convolution. (b)–(c) SVOCT images with full spectral band and 1/4 spectral band, respectively. (d) Mask of dynamic vascular signals (red) and static signals (blue) in the magnified local region in (a)–(f) for SNR calculation. (e)–(g) Histograms of dynamic vascular pixel intensities (red) and background static pixel intensities (blue). The depth-range of 0–130 μm (with tissue refractive index of 1.35) below surface is used for (a)–(c) and (a)–(c) share the same scale bar.

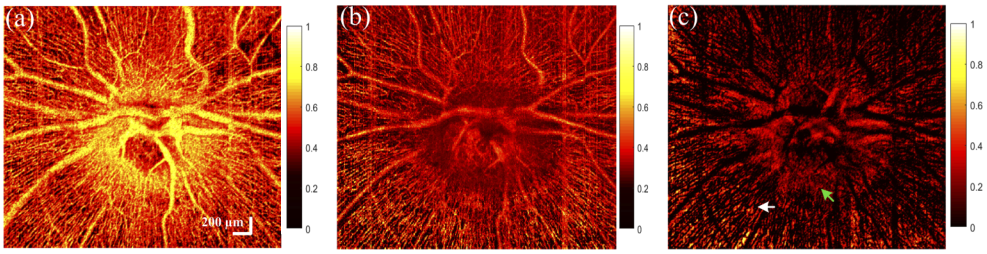

Fig. 7. Comparison of GOCTA' image with SVOCT image of optic nerve head region. (a) GOCTA' image with 1/4 spectral band and skipped convolution. (b) SVOCT image of the same region with full spectral range. (c) Difference image between GOCTA' and SVOCT. Green arrow: More microvasculature in lamina cribrosa. White arrow: More microvasculature in the periphery of lamina cribrosa. The depth-range of 0–170 μm (with tissue refractive index of 1.35) below surface is used and (a)–(c) share the same scale bar.

Biomedical Optics EXPRESS

Table 3. 3D (608 × 2048 × 304 pixels) data processing time for SVOCT and GOCTA' on CPU or GPU

	3D data processing time (s)		
	SVOCT (Full spectral band)	SVOCT (1/4 spectral band)	GOCTA'
CPU	141.2	29.8	0.98
GPU	-	-	0.25

4. Discussion and conclusion

In this manuscript, we systematically analyzed the effect of reducing input data volume and skipped convolution for GOCTA' processing with an aim to improve the image processing speed and minimize loss of image quality, using healthy human retinal OCT datasets (608×2048×304 pixels). Overall speed improvement of as high as 29.8 times was achieved over SVOCT with 1/4 spectral band. The speed advantage of GOCTA' is achieved by two main factors: no k-space re-sampling and skipped convolution. In this work, the size of Gabor filter kernel in all *in vivo* experiments is 16 pixels.

In Table 1, only three different A-scan pixel sizes (2048, 1024, 512) are used to calculate computational complexity for comparison. To explore the improvement of computational complexity with different A-scan pixel sizes, we calculated the computational complexity of from 256 to 32768 pixels and the results are shown in Fig. 8. We can see that the computational complexity improvement achieved by skipped convolution over FFT increases non-linearly with the increase of the A-scan pixel number.

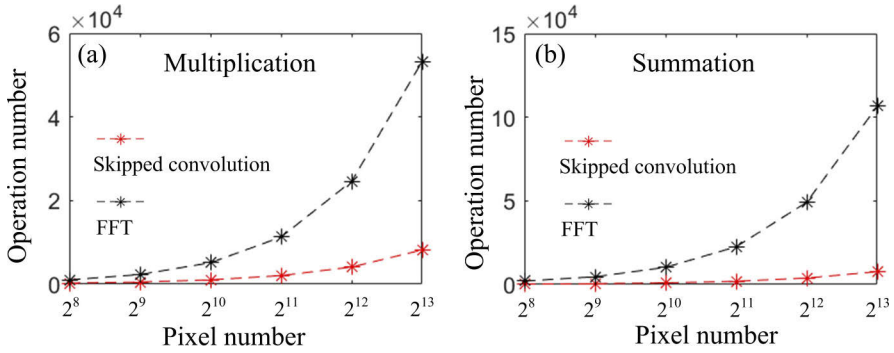

Fig. 8. The comparison of computational complexity between skipped convolution and FFT, (a) multiplication and (b) summation. The operation numbers are calculated based on different A-scan pixel numbers with Gabor filters of 16 pixels.

The significant processing speed improvement may allow new workflow of ophthalmological OCT imaging. In particular, real-time GOCTA' imaging, inherently associated with less motion artifacts, may be performed as the screening step for identification of suspected patient or retinal region for more detailed imaging or analysis. Even more interesting is the fact that excellent quality GOCTA' images of the retinal microvasculature can be obtained with substantially narrower OCT system optical bandwidth. The numerical analysis presented here may guide future OCTA hardware design and help with system cost reduction.

One limitation of GOCTA' algorithm is that image or feature alignment in the spatial domain along the A-scan direction is not directly feasible without FFT or other steps with similar computational complexity, as GOCTA' is directly performed on spectral fringes to calculate microvascular images. Therefore, different motion artifact suppression techniques would be required, such as 2D based algorithms [26,27]. Because the model of GOCTA signal versus

Biomedical Optics EXPRESS

displacements is an oscillation pattern, the capability of differentiating blood flow velocities by GOCTA intensity cannot be achieved.

Finally, the speed advantage of GOCTA' is achieved by avoiding k-space re-sampling and performing FFT in the depth direction. Therefore, depth resolved structural information is not inherently available in GOCTA' processing. Although by choosing appropriate Gabor filter parameters, different layers of microvasculature of the retina can be distinguished, such operations require *a priori* information of the depths of the layers and therefore only appropriate for normal subjects. Pathological subjects may have layer disruption and therefore, GOCTA' can potentially serve as a screening technique to identify images which deviate away from an expected range of normal subjects. Furthermore, the standard FFT based data processing method can also be performed on the saved data for more detailed analysis after detecting abnormal vascular distribution.

In summary, we optimized our proposed Gabor optical coherence tomographic angiography (GOCTA) algorithm to achieve better image quality, investigated the model of optimized GOCTA' signals versus moving velocities of scattering particles and further optimized GOCTA' on data processing speed in this manuscript. By using 1/4 spectral band and skipped convolution, data processing speed for 3D dataset is 30 times faster than SVOCT with the same spectral bandwidth. And compared to our previous work [24], data processing speed is improved of about 26.7 times and 34 times for 3D dataset on CPU and GPU, respectively. The proposed algorithm can provide depth dependent microvasculature images in multiple layers using *a priori* information, and this algorithm could be especially suitable for SDOCT systems with ultra-high A-scan speed or wide scanning range, where angiographic processing of large quantity of datasets are required.

Funding

Natural Sciences and Engineering Research Council of Canada.

Disclosures

The authors declare that there are no conflicts of interest related to this work.

References

1. D. Huang, E. A. Swanson, C. P. Lin, J. S. Schuman, W. G. Stinson, W. Chang, M. R. Hee, T. Flotte, K. Gregory, C. A. Puliafito, and J. G. Fujimoto, "Optical coherence tomography," Science **254**(5035), 1178–1181 (1991).
2. Z. Chen, T. E. Milner, S. Srinivas, X. Wang, A. Malekafzali, M. J. C. van Gemert, and J. Stuart Nelson, "Noninvasive imaging of in vivo blood flow velocity using optical Doppler tomography," Opt. Lett. **22**(14), 1119–1121 (1997).
3. V. X. D. Yang, M. L. Gordon, B. Qi, J. Pekar, S. Lo, E. Seng-Yue, A. Mok, B. C. Wilson, and I. A. Vitkin, "High speed, wide velocity dynamic range Doppler optical coherence tomography (Part I): System design, signal processing, and performance," Opt. Express **11**(7), 794–809 (2003).
4. J. A. Izatt, M. D. Kulkarni, S. Yazdanfar, J. K. Barton, and A. J. Welch, "*In vivo* bidirectional color Doppler flow imaging of picoliter blood volumes using optical coherence tomography," Opt. Lett. **22**(18), 1439–1441 (1997).
5. Y. H. Zhao, Z. P. Chen, C. Saxer, Q. M. Shen, S. H. Xiang, J. F. de Boer, and J. S. Nelson, "Doppler standard deviation imaging for clinical monitoring of in vivo human skin blood flow," Opt. Lett. **25**(18), 1358–1360 (2000).
6. G. Liu, L. Chou, W. Jia, W. Qi, B. Choi, and Z. Chen, "Intensity-based modified Doppler variance algorithm: application to phase instable and phase stable optical coherence tomography systems," Opt. Express **19**(12), 11429–11440 (2011).
7. R. K. Wang, S. L. Jacques, Z. Ma, S. Hurst, S. R. Hanson, and A. Gruber, "Three Dimensional Optical Angiography," Opt. Express **15**(7), 4083–4097 (2007).
8. J. Fingler, D. Schwartz, C. Yang, and S. E. Fraser, "Mobility and transverse flow visualization using phase variance contrast with spectral domain optical coherence tomography," Opt. Express **15**(20), 12636–12653 (2007).
9. J. Barton and S. Stromski, "Flow measurement without phase information in optical coherence tomography images," Opt. Express **13**(14), 5234–5239 (2005).
10. A. Mariampillai, B. A. Standish, E. H. Moriyama, M. Khurana, N. R. Munce, M. K. K. Leung, J. Jiang, A. Cable, B. C. Wilson, I. A. Vitkin, and V. X. D. Yang, "Speckle variance detection of microvasculature using swept-source optical coherence tomography," Opt. Lett. **33**(13), 1530–1532 (2008).
11. A. Mariampillai, M. K. K. Leung, M. Jarvi, B. A. Standish, K. Lee, B. C. Wilson, A. Vitkin, and V. X. D. Yang, "Optimized speckle variance OCT imaging of microvasculature," Opt. Lett. **35**(8), 1257–1259 (2010).

Biomedical Optics EXPRESS

12. C. Chen, K. H. Y. Cheng, R. Jakubovic, J. Jivraj, J. Ramjist, R. Deorajh, W. Gao, E. Barnes, L. Chin, and V. X. D. Yang, "High speed, wide velocity dynamic range Doppler optical coherence tomography (Part V): Optimal utilization of multi-beam scanning for Doppler and speckle variance microvascular imaging," Opt. Express **25**(7), 7761–7777 (2017).
13. J. Enfield, E. Jonathan, and M. Leahy, "In vivo imaging of the microcirculation of the volar forearm using correlation mapping optical coherence tomography (cmOCT)," Biomed. Opt. Express **2**(5), 1184–1193 (2011).
14. C. Chen, W. Shi, and W. Gao, "Imaginary part-based correlation mapping optical coherence tomography for imaging of blood vessels in vivo," J. Biomed. Opt. **20**(11), 116009 (2015).
15. C. Chen, J. Liao, and W. Gao, "Cube data correlation-based imaging of small blood vessels," Opt. Eng. **54**(4), 043104 (2015).
16. Y. Jia, O. Tan, J. Tokayer, B. Potsaid, Y. Wang, J. J. Liu, M. F. Kraus, H. Subhash, J. G. Fujimoto, J. Hornegger, and D. Huang, "Split-spectrum amplitude-decorrelation angiography with optical coherence tomography," Opt. Express **20**(4), 4710–4725 (2012).
17. W. Shi, W. Gao, C. Chen, and V. X. D. Yang, "Differential standard deviation of log-scale intensity based optical coherence tomography angiography," J. Biophotonics **10**(12), 1597–1606 (2017)..
18. L. An, J. Qin, and R. K. Wang, "Ultrahigh sensitive optical microangiography for in vivo imaging of microcirculations within human skin tissue beds," Opt. Express **18**(8), 8220–8228 (2010).
19. S. Yousefi, J. Qin, and R. K. Wang, "Super-resolution spectral estimation of optical micro-angiography for quantifying blood flow within microcirculatory tissue beds in vivo," Biomed. Opt. Express **4**(7), 1214–1228 (2013).
20. J. Barrick, A. Doblas, M. R. Gardner, P. R. Sears, L. E. Ostrowski, and A. L. Oldenburg, "High-speed and high-sensitivity parallel spectral-domain optical coherence tomography using a supercontinuum light source," Opt. Lett. **41**(24), 5620–5623 (2016).
21. B. Grajciar, Y. Lehareinger, A. F. Fercher, and R. A. Leitgeb, "High sensitivity phase mapping with parallel Fourier domain optical coherence tomography at 512 000 A-scan/s," Opt. Express **18**(21), 21841–21850 (2010).
22. O. P. Kocaoglu, T. L. Turner, Z. Liu, and D. T. Miller, "Adaptive optics optical coherence tomography at 1 MHz," Biomed. Opt. Express **5**(12), 4186–4200 (2014).
23. J. Xu, W. Wei, S. Song, X. Qi, and R. K. Wang, "Scalable wide-field optical coherence tomography-based angiography for *in vivo* imaging applications," Biomed. Opt. Express **7**(5), 1905–1919 (2016).
24. C. Chen and V. X. D. Yang, "Gabor optical coherence tomographic angiography (GOCTA) (Part I): human retinal imaging *in vivo*," Biomed. Opt. Express **8**(12), 5724–5734 (2017).
25. R. Leitgeb, C. K. Hitzenberger, and A. F. Fercher, "Performance of fourier domain vs. time domain optical coherence tomography," Opt. Express **11**(8), 889–894 (2003).
26. M. Heisler, S. Lee, Z. Mammo, Y. Jian, M. Ju, A. Merkur, E. Navajas, C. Balaratnasingam, M. F. Beg, and M. V. Sarunic, "Strip-based registration of serially acquired optical coherence tomography angiography," J. Biomed. Opt. **22**(3), 036007 (2017).
27. P. Zang, G. Liu, M. Zhang, C. Dongye, J. Wang, A. D. Pechauer, T. S. Hwang, D. J. Wilson, D. Huang, D. Li, and Y. Jia, "Automated motion correction using parallel-strip registration for wide-field *en face* OCT angiogram," Biomed. Opt. Express **7**(7), 2823–2836 (2016).